DELPHI Collaboration

DELPHI 2000-128 CONF 427
1 July, 2000

Results on Fermion-Pair Production at LEP running from 192 to 202 GeV

A.Behrmann[1], I.Boyko[2], P.Checchia[3], G.Della Ricca[4], I.Gouz[5], J.Holt[6], M.Nikolenko[2], A.Olchevski[2], M.Paganoni[3], D.Reid[7], P.Renton[6], G.Morton[6], T.Myklebust[8], G.R.Wilkinson[6], M.Winter[9], V.Zhuravlov[2]

Abstract

A preliminary analysis of the data collected in 1999 with the DELPHI detector at e^+e^- collision energy between 192 and 202 GeV was performed in order to extract the hadronic and leptonic cross-sections, as well as the leptonic forward-backward asymmetries.
Various interpretations of the results, including possible physics beyond the Standard Model, are presented. In particular, the data are used to investigate potential contact interactions, the exchange of sneutrinos in R-parity violating SUSY and for $Z^{'}$ bosons and search for the existence of gravity in extra dimensions.

Contributed Paper for ICHEP2000

[1]Fachbereich Physik, University of Wuppertal, Wuppertal, FRG
[2]Joint Institute for Nuclear Research, Dubna, Russia
[3]INFN, Padova, Italy
[4]INFN, Trieste, Italy
[5]INFN, Milano, Italy
[6]Department of Physics, University of Oxford, Oxford,UK
[7]NIKHEF, Postbus 41882, NL-1009 DB Amsterdam, The Netherlands
[8]University of Oslo, Institute of Physics, Oslo, Norway
[9]Institut de Recherches Subatomiques, IN2P3-CNRS/ULP, Strasbourg, France

1 Introduction

Preliminary results are presented from the analyses of fermion–pair final states collected in 1999 with the DELPHI experiment [1] at centre–of–mass energies, $\sqrt{s}$, between 192 and 202 GeV. Measurements of cross–sections for inclusive hadronic, electron–pair, muon–pair and tau–pair final states are given, together with leptonic forward–backward asymmetries. These results complement those obtained from data collected from 1995 to 1998 at lower collision energies from 130 to 189 GeV [2, 3]. Polar angle distributions of $\mu^+\mu^-$ and $\tau^+\tau^-$ events are also given, adding to the results given in [3].

The measurements of the cross–sections and forward–backward asymmetries together with the results presented in [2, 3] and from LEP running in the vicinity of the Z–resonance [4, 5], are used to update the searches for new physics involving contact interactions, R-parity violating SUSY, and additional neutral gauge bosons given in [2, 3]. The data is also used to search for effects of gravity in theories with extra dimensions, updating the results given in [3]. For the theoretical motivation and technical details, the reader is referred to [2, 3].

Results on fermion–pair production at LEP at collision energies from 130 to 189 GeV from the other LEP collaborations can be found in [6], together with limits derived from these results.

The measurements of cross–sections, forward–backward asymmetries and angular distributions are given in section 2. The interpretations of the data are presented in section 3. A summary and conclusions are given in section 4.

2 Measurements of cross–sections and asymmetries

The luminosity analysis of the data collected during LEP operation in 1999 followed closely the one described in [2, 3]. The total experimental systematic uncertainty on the integrated luminosity determination amounts to 0.50%, to be combined with a 0.25% uncertainty reflecting the precision of the theoretical calculations underlying the computation of the cross–section visible in the luminometers. The errors are to be added in quadrature to the other sources of systematics uncertainty given below.

The luminosities used for the analysis of the inclusive hadronic final states and estimates of the mean centre–of–mass energy GeV [7] are given in Table 1. There are small differences in the luminosities and mean centre–of–mass energies for the other channels , due to the selection of different running periods for analysis, based on the performance of the subdetectors of DELPHI.

As in [2, 3], the cross–sections and asymmetry measurements are given for different ranges of the reduced centre–of-mass energy, $\sqrt{s'}$: for hadronic final states an *inclusive* sample, defined as $\sqrt{s'}/\sqrt{s} > 0.10$, and a *non–radiative* sample, defined as $\sqrt{s'}/\sqrt{s} > 0.85$; for muon and tau final states an *inclusive* sample with $\sqrt{s'} > 75\,\mathrm{GeV}$, and a *non–radiative* sample with $\sqrt{s'}/\sqrt{s} > 0.85$. For electron final states, a cut on the acollinearity[1] angle between the electrons, $\theta_{acol} < 20^\circ$, was applied, corresponding approximately to a cut of $\sqrt{s'}/\sqrt{s} > 0.85$. The number of events selected for each final state are given in Table 2.

[1]The acollinearity angle between two particles is defined as $\cos\theta_{acol} = -p_1.p_2/|p_1||p_2|$, where p_1 and p_2 are the 3–momenta of the particles.

The results on the cross section and leptonic forward–backward asymmetry measurements presented in this section are from the analyses of e^+e^-, $\mu^+\mu^-$, $\tau^+\tau^-$ and inclusive hadronic final states. These analyses were similar to the ones performed at lower energies and the details, such as event selection and reduced energy ($\sqrt{s'}$) determination can be found, in [2, 3].

The distributions of $\sqrt{s'}/\sqrt{s}$ obtained for the real and the simulated data are shown in Figure 1 for the hadronic channel and Figure 2 for the muon and tau channels. The methods of estimating $\sqrt{s'}$ correspond to slightly different definitions of this variable. For $\mu^+\mu^-$ and the $\tau^+\tau^-$ final states, $\sqrt{s'}$ is the invariant mass of the muons or tau-leptons in the final state. For the inclusive hadronic final states, the estimated $\sqrt{s'}$ can be considered in theoretical predictions to be the invariant mass of the s-channel propagator.

For the $\mu^+\mu^-$ and $\tau^+\tau^-$ final states, the cross-sections and asymmetries were extrapolated to 4π acceptance using samples of events generated with KORALZ [12]. In the calculations of KORALZ there is no interference between Initial State and Final State Radiation. Corrections to the extrapolation for this interference were determined using the semi-analytical calculations of ZFITTER [13], in which the interference was computed to $\mathcal{O}(\alpha)$, and applied to the results. To account for missing higher order corrections, a systematic uncertainty of half the correction was taken. For the inclusive hadronic states, any correction for the interference between initial and final state radiation was estimated to be negligibly small within the precision of the measurement.

The measured cross–sections and forward–backward asymmetries for the different final states, and the theoretical expectations, for collisions energies from 192 to 202 GeV as given in Table 4 Figures 3 shows the measured hadron, electron–pair, muon–pair and tau–pair cross–sections for all collision energies ranging from 130 up to 202 GeV from DELPHI. The forward–backward asymmetries for electron–pairs, muon–pairs and tau–pairs are shown in Figure 4. The differences between the measured cross–sections and forward–backward asymmetries and the SM predictions for non–radiative samples in the different channels are shown in figures 5 and 6. The SM prediction are from the TOPAZ0 program [14] for electron final states and the ZFITTER program [13] for the others.

Statistical uncertainties and systematic errors due to the event selection and to the residual background subtraction are shown in Table 3. For the cross–section measurements, they are to be added in quadrature to the uncertainty coming from the luminosity determination. The uncertainties on the theoretical predictions for the s-channels $e^+e^-\to\mu^+\mu^-$, $e^+e^-\to\tau^+\tau^-$ and inclusive hadronic cross-sections are estimated to be below 1%.

In addition to the measurements of the cross–sections and asymmetries, measurements of the differential cross–sections, $d\sigma/d\cos\theta$, are measured for the $\mu^+\mu^-$ and $\tau^+\tau^-$ final states for the *non–radiative* samples. The results are given in Table 5 and 6 respectively for $\mu^+\mu^-$ and $\tau^+\tau^-$ final states. For the $\mu^+\mu^-$ final states, the scattering angle θ is the angle of the negative fermion with respect to the incoming electron in the laboratory frame. For the $\tau^+\tau^-$ final states, the angle is defined as in [3]. The weighted average of the differential cross–sections for $\sqrt{s} \sim 192 - 202\,\mathrm{GeV}$ for $\mu^+\mu^-$ and $\tau^+\tau^-$ final states are shown in Figure 7. The Standard Model expectations evaluated with ZFITTER at the average centre-of-mass energy are shown for comparison.

Overall, no substantial departure of the measurements from the Standard Model predictions was found.

	Collision Energy (GeV)			
	~ 192	~ 196	~ 200	~ 202
Luminosity (pb^{-1})	25.11	76.13	82.96	40.28
Energy (GeV)	191.58	195.51	199.51	201.64

Table 1: The luminosities and collision energies for the inclusive hadronic final states

Channel	Collision Energy (GeV)			
	~ 192	~ 196	~ 200	~ 202
$e^+e^- \to q\bar{q}(\gamma)$	2438	7291	7501	3588
$e^+e^- \to e^+e^-(\gamma)$	533	1573	1557	783
$e^+e^- \to \mu^+\mu^-(\gamma)$	161	382	506	207
$e^+e^- \to \tau^+\tau^-(\gamma)$	78	228	225	109

Table 2: The statistics used in the analyses of the different final states. For each channel, the values refer to the samples with $\sqrt{s'/s} > 0.10$ for hadrons, $\sqrt{s'} > 75$ for muons and taus and $\theta_{acol} < 20^\circ$ for electrons.

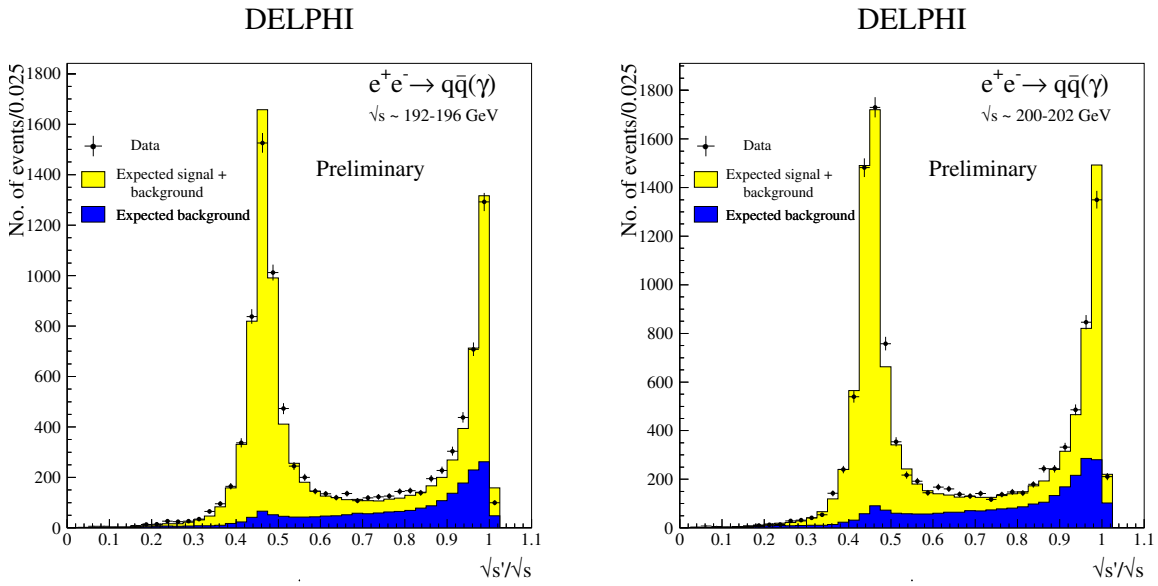

Figure 1: Combined distributions of the reconstructed reduced energy for the $e^+e^- \to q\bar{q}(\gamma)$ process at $\sqrt{s} \sim 192$ and 196 GeV and at $\sqrt{s} \sim 200$ and 202 GeV. The points show the real data, and the histograms show the simulated signal and background samples. The expected signals are simulated with the PYTHIA [8] generator and are normalised to the luminosities of the data set analysed. Differences between data and simulation in the shape of these distributions are taken into account when determining the systematic errors on the measured cross–sections.

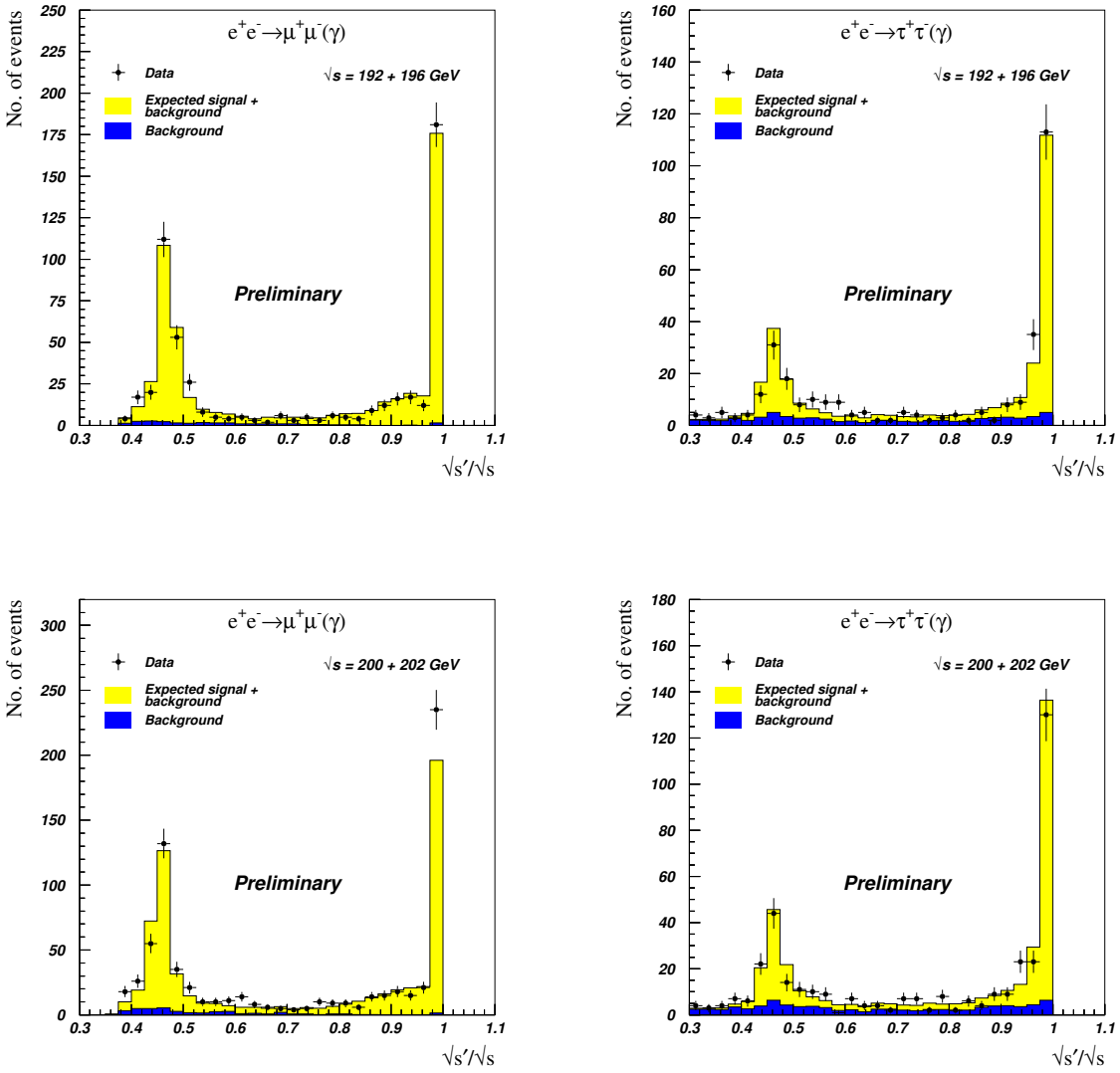

Figure 2: Combined distributions of the reconstructed reduced energy for the $e^+e^- \to \mu^+\mu^-(\gamma)$ and $e^+e^- \to \tau^+\tau^-(\gamma)$ processes at $\sqrt{s} \sim 192$ and 196 GeV and at $\sqrt{s} \sim 200$ and 202 GeV. The points stand for the data and the histograms represent the signal and background. The expected signals are simulated with the KORALZ [12] generator scaled to the ZFITTER [13] predictions and are normalised to the luminosities of the data sets analysed.

Non–radiative								
$\sqrt{s}$		$\Delta\sigma^h/\sigma^h$	$\Delta\sigma^e/\sigma^e$	$\Delta\sigma^\mu/\sigma^\mu$	$\Delta\sigma^\tau/\sigma^\tau$	$\Delta A_{FB}{}^e$	$\Delta A_{FB}{}^\mu$	$\Delta A_{FB}{}^\tau$
GeV		%	%	%	%	10^{-3}	10^{-3}	10^{-3}
~ 192	(stat.)	4.9	4.3	12.8	19.4	23	102	177
	(syst.)	2.1	1.0	3.4	4.9	$^{+10}_{-3}$	3	40
~ 196	(stat.)	2.9	2.5	7.4	10.2	15	60	88
	(syst.)	2.1	1.0	3.3	5.1	$^{+10}_{-3}$	3	40
~ 200	(stat.)	2.9	2.5	6.6	10.4	16	55	87
	(syst.)	2.3	1.1	3.3	4.8	$^{+10}_{-3}$	3	40
~ 202	(stat.)	4.2	3.5	10.8	15.1	20	89	129
	(syst.)	2.6	1.1	3.4	5.2	$^{+10}_{-3}$	3	40

Inclusive								
$\sqrt{s}$		$\Delta\sigma^h/\sigma^h$	$\Delta\sigma^e/\sigma^e$	$\Delta\sigma^\mu/\sigma^\mu$	$\Delta\sigma^\tau/\sigma^\tau$	$\Delta A_{FB}{}^e$	$\Delta A_{FB}{}^\mu$	$\Delta A_{FB}{}^\tau$
GeV		%	%	%	%	10^{-3}	10^{-3}	10^{-3}
~ 192	(stat.)	2.5	–	7.9	14.1	–	76	147
	(syst.)	1.6	–	3.4	6.0	–	2	40
~ 196	(stat.)	1.4	–	5.1	8.2	–	49	84
	(syst.)	1.5	–	3.4	6.0	–	2	40
~ 200	(stat.)	1.4	–	4.4	7.8	–	42	78
	(syst.)	1.7	–	3.4	5.9	–	3	40
~ 202	(stat.)	2.1	–	6.9	12.8	–	65	124
	(syst.)	1.8	–	3.4	6.1	–	5	40

Table 3: Statistical and systematic uncertainties of the total and non–radiative cross section and forward–backward asymmetry measurements for the different final states. "Non–radiative" refers to $\sqrt{s'}/\sqrt{s} > 0.85$ for muon, tau and hadronic final states, and $\theta_{acol} < 20^\circ$ for electron pairs. "Inclusive" refers to $\sqrt{s'}/\sqrt{s} > 0.10$ for the hadronic final states and to $\sqrt{s'} > 75$ GeV for the muon and tau final states. The luminosity uncertainties (0.50% experimental and 0.25% theoretical) are not included.

Energy (GeV)		~ 192	~ 196	~ 200	~ 202
σ_{had} (pb)	$\sqrt{s'}/\sqrt{s} > 0.85$	21.5 ± 1.1	21.2 ± 0.6	19.2 ± 0.6	19.4 ± 0.8
	Theory	21.2	20.0	19.0	18.5
	$\sqrt{s'}/\sqrt{s} > 0.10$	93.3 ± 2.3	92.7 ± 1.3	86.3 ± 1.2	85.0 ± 1.8
	Theory	93.6	89.1	84.8	82.7
$\sigma_{\mu\mu}$ (pb)	$\sqrt{s'}/\sqrt{s} > 0.85$	2.70 ± 0.34	2.77 ± 0.20	3.08 ± 0.20	2.36 ± 0.26
	Theory	2.97	2.84	2.72	2.65
	$\sqrt{s'}/\sqrt{s} > 0.10$	7.23 ± 0.57	5.96 ± 0.31	6.99 ± 0.31	5.81 ± 0.40
	Theory	6.90	6.60	6.32	6.17
$\sigma_{\tau\tau}$(pb)	$\sqrt{s'}/\sqrt{s} > 0.85$	2.47 ± 0.48	2.94 ± 0.30	2.69 ± 0.28	2.51 ± 0.38
	Theory	3.03	2.89	2.77	2.71
	$\sqrt{s'}/\sqrt{s} > 0.10$	6.46 ± 0.91	6.19 ± 0.51	6.40 ± 0.50	5.25 ± 0.67
	Theory	6.89	6.56	6.26	6.12
$A_{FB}{}^{\mu}$	$\sqrt{s'}/\sqrt{s} > 0.85$	0.608 ± 0.102	0.582 ± 0.060	0.565 ± 0.055	0.579 ± 0.089
	Theory	0.584	0.581	0.577	0.575
	$\sqrt{s'}/\sqrt{s} > 0.10$	0.297 ± 0.076	0.304 ± 0.049	0.318 ± 0.042	0.353 ± 0.065
	Theory	0.315	0.315	0.314	0.313
$A_{FB}{}^{\tau}$	$\sqrt{s'}/\sqrt{s} > 0.85$	0.608 ± 0.102	0.582 ± 0.060	0.565 ± 0.055	0.579 ± 0.089
	Theory	0.584	0.581	0.577	0.575
	$\sqrt{s'}/\sqrt{s} > 0.10$	0.297 ± 0.076	0.304 ± 0.049	0.318 ± 0.042	0.353 ± 0.065
	Theory	0.315	0.315	0.314	0.313
σ_{ee} (pb)	$\theta_{acol} < 20^{\circ}$	24.03 ± 1.03	22.43 ± 0.56	20.56 ± 0.51	21.30 ± 0.75
	Theory	22.29	21.36	20.52	20.08
$A_{FB}{}^{e}$	$\theta_{acol} < 20^{\circ}$	0.831 ± 0.024	0.818 ± 0.015	0.789 ± 0.016	0.829 ± 0.020
	Theory	0.823	0.823	0.823	0.823

Table 4: Results of the cross–section and asymmetry measurements for the different final states. The errors indicated are statistical only. Systematic errors related to the event selection and residual backgrounds are provided in Table 3. Those coming from the luminosity determination are given in the text. The theoretical prediction is also indicated. The hadronic, muon and tau results are corrected for all cuts, apart from the $\sqrt{s'}$ cut.

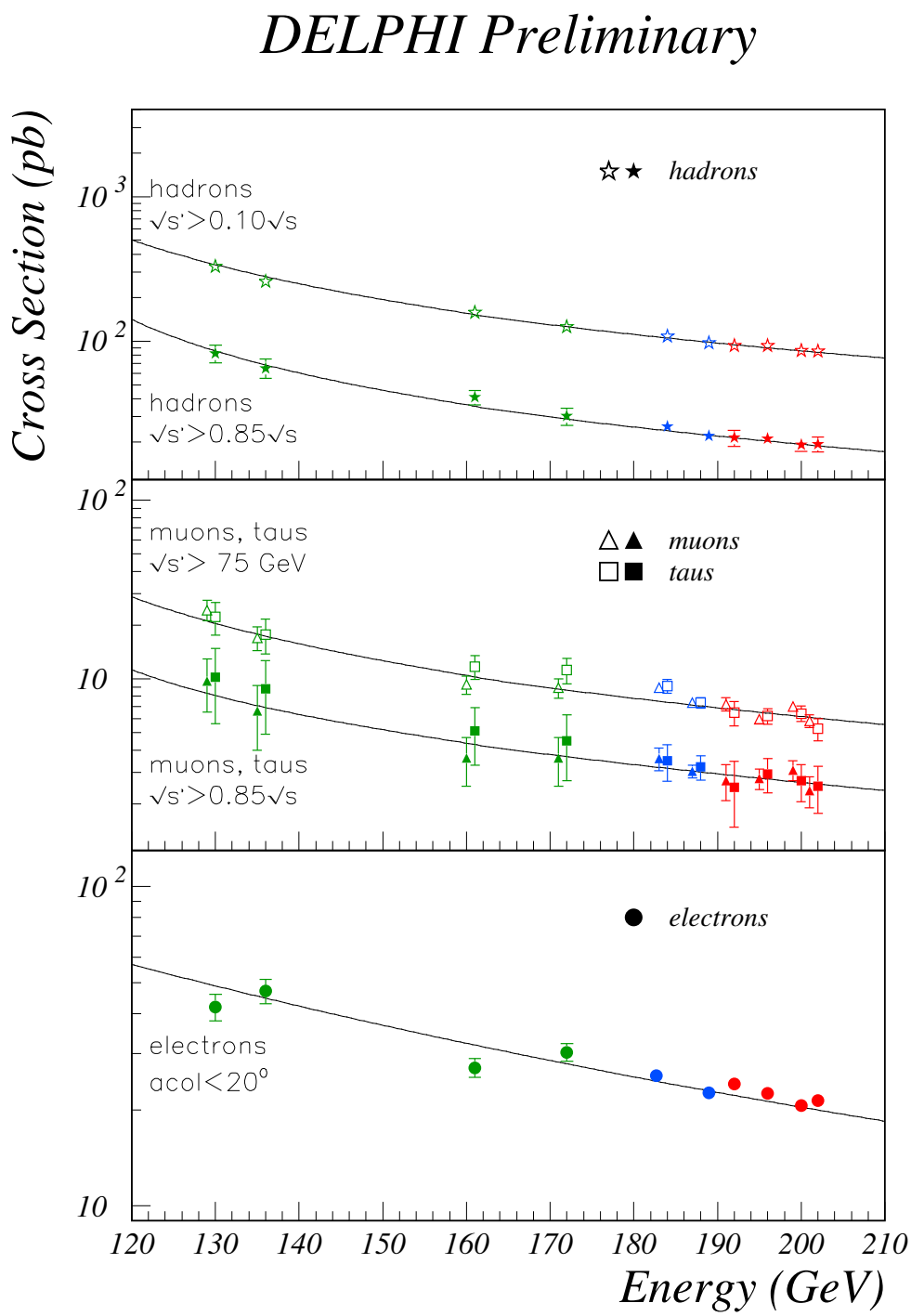

Figure 3: Cross–sections for the $e^+e^- \to q\bar{q}(\gamma)$, $\mu^+\mu^-(\gamma)$ and $\tau^+\tau^-(\gamma)$, and $e^+e^- \to e^+e^-(\gamma)$ processes measured at energies from 130 up to 202 GeV. The curves show the SM prediction of the TOPAZ0 program [14] for electron final states and the ZFITTER program [13] for the other final states. Open points represent the *inclusive* selections and solid points the *non–radiative* selections.

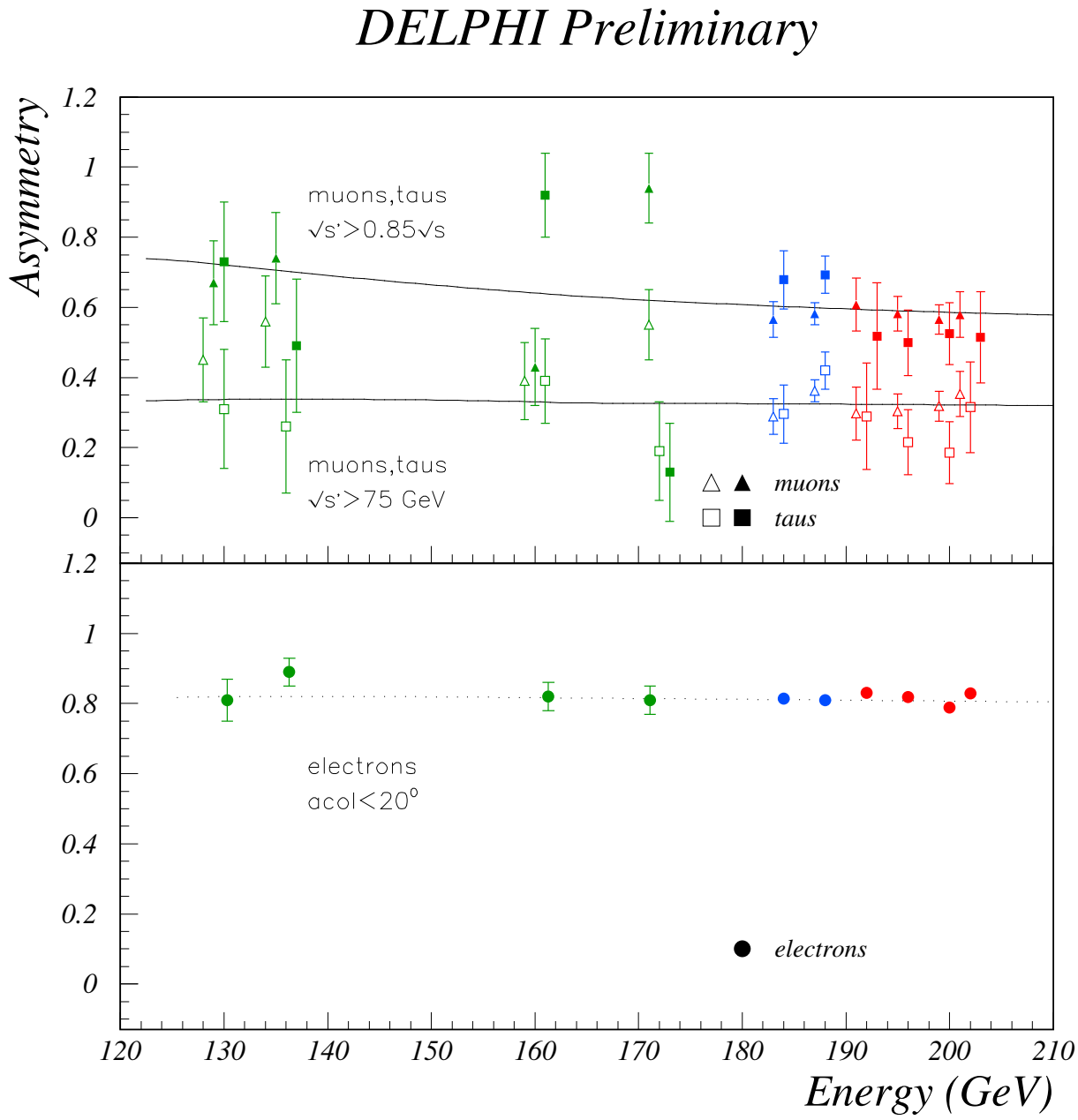

Figure 4: The forward–backward charge asymmetries in the reactions $e^+e^- \to \mu^+\mu^-(\gamma)$ and $\tau^+\tau^-(\gamma)$, and $e^+e^-(\gamma)$ measured at energies ranging from 130 to 202 GeV. The curves show the SM prediction of the TOPAZ0 program [14] for electron final states and the ZFITTER program [13] for the other final states. Open points represent the *inclusive* selections and solid points the *non–radiative* selections.

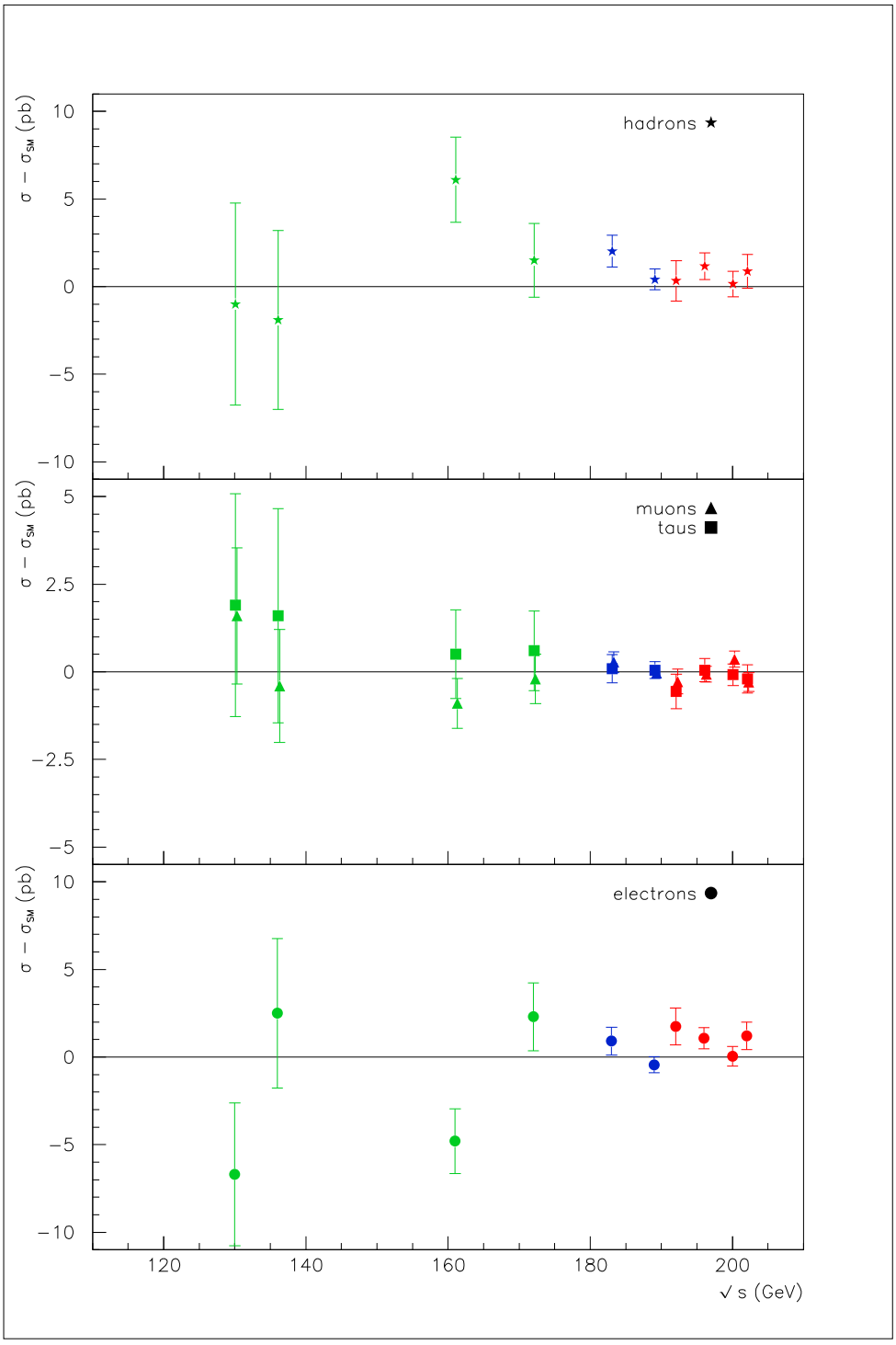

Figure 5: The differences between measured cross–sections and SM predictions for the *non-radiative* event samples in the $e^+e^- \to q\bar{q}(\gamma)$, $\mu^+\mu^-(\gamma)$ and $\tau^+\tau^-(\gamma)$, and $e^+e^- \to e^+e^-(\gamma)$ channels, at energies from 130 up to 202 GeV. The SM prediction are calculated with TOPAZ0 program [14] for electron final states and the ZFITTER program [13] for the other final states.

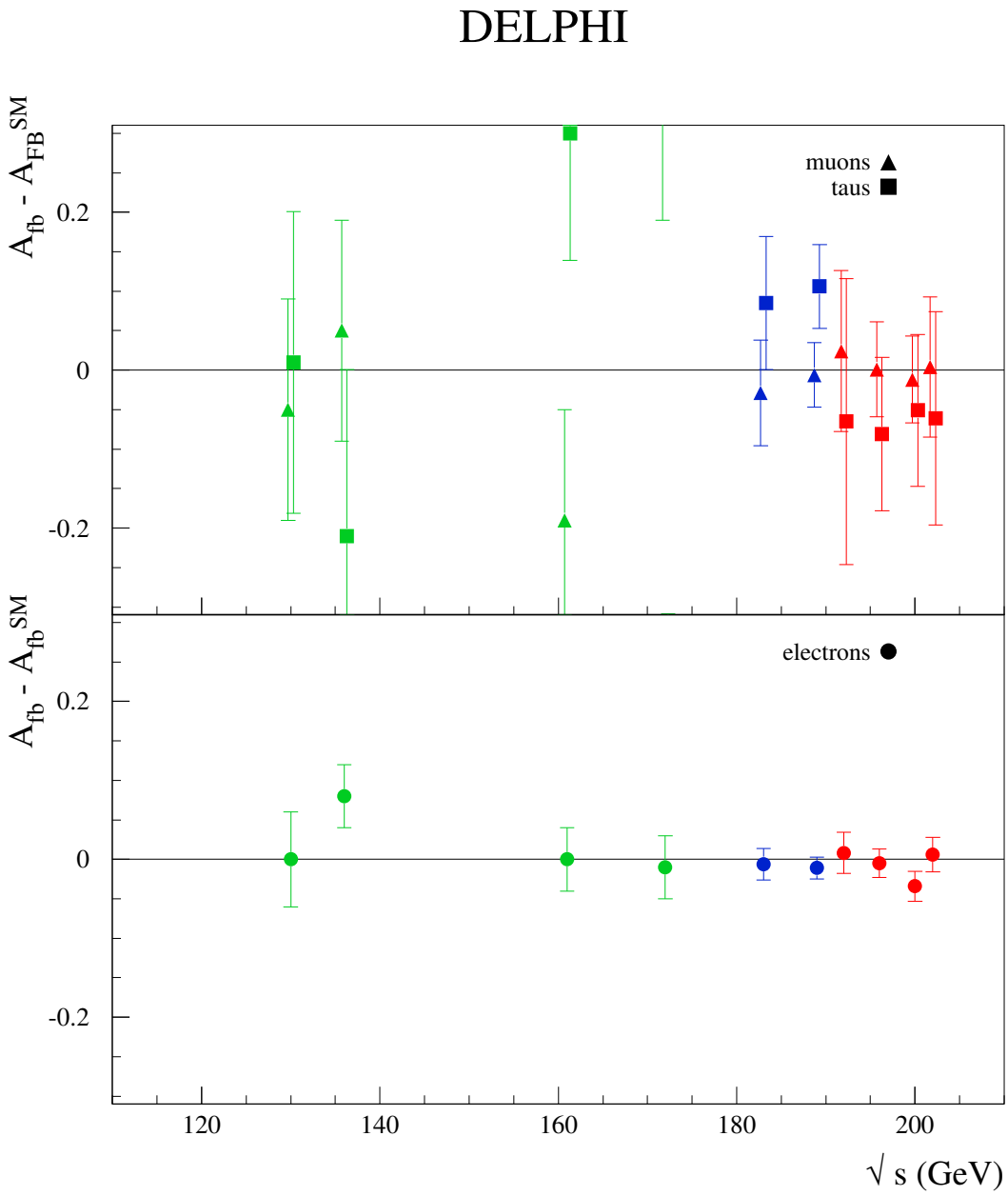

Figure 6: The differences between measured forward–backward asymmetries and SM predictions for *non-radiative* event samples in the $e^+e^- \to q\bar{q}(\gamma)$, $\mu^+\mu^-(\gamma)$ and $\tau^+\tau^-(\gamma)$, and $e^+e^- \to e^+e^-(\gamma)$ channels, at energies from 130 up to 202 GeV. The SM prediction are calculated with TOPAZ0 program [14] for electron final states and the ZFITTER program [13] for the other final states.

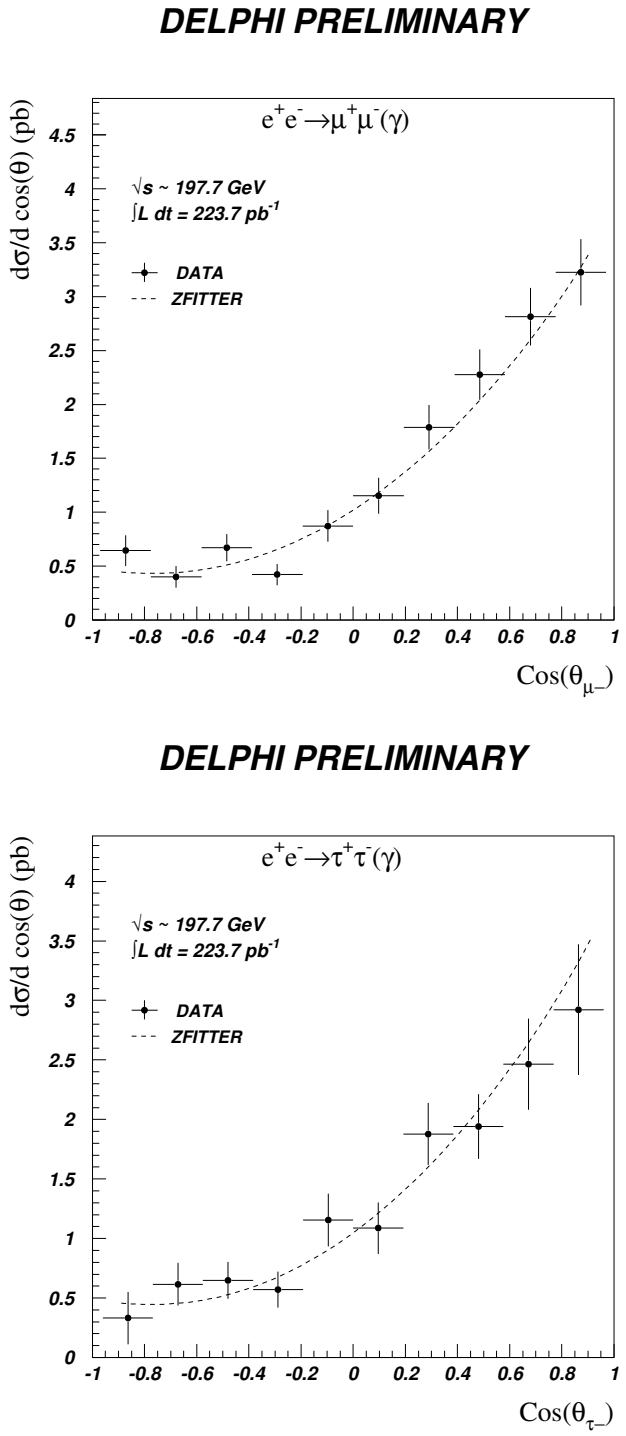

Figure 7: The weighted average of the differential cross-sections for measurements at $\sqrt{s} \sim 192-202\,\mathrm{GeV}$ for $\mu^+\mu^-$ and $\tau^+\tau^-$ final states. Also shown are the SM expectations calculated from ZFITTER for the differential cross–sections at the average value of $\sqrt{s}$

$e^+e^- \to \mu^+\mu^-$ ($\sqrt{s} \sim 192$ GeV)		
	$d\sigma/d\cos\theta$ (pb)	
$\cos\theta$	Theory	Measurement
[-0.97,-0.80]	0.460	0.000±0.331±0.005
[-0.80,-0.60]	0.459	0.202±0.202±0.005
[-0.60,-0.40]	0.533	0.814±0.407±0.020
[-0.40,-0.20]	0.693	0.385±0.272±0.009
[-0.20, 0.00]	0.941	1.068±0.477±0.027
[0.00, 0.20]	1.280	0.619±0.357±0.016
[0.20, 0.40]	1.712	2.595±0.720±0.063
[0.40, 0.60]	2.240	1.859±0.620±0.046
[0.60, 0.80]	2.873	2.592±0.748±0.067
[0.80, 0.97]	3.661	3.191±0.885±0.080

$e^+e^- \to \mu^+\mu^-$ ($\sqrt{s} \sim 196$ GeV)		
	$d\sigma/d\cos\theta$ (pb)	
$\cos\theta$	Theory	Measurement
[-0.97,-0.80]	0.450	0.716±0.253±0.018
[-0.80,-0.60]	0.447	0.520±0.196±0.013
[-0.60,-0.40]	0.515	0.614±0.205±0.015
[-0.40,-0.20]	0.665	0.208±0.120±0.005
[-0.20, 0.00]	0.900	0.875±0.253±0.022
[0.00, 0.20]	1.221	1.459±0.318±0.035
[0.20, 0.40]	1.632	1.279±0.301±0.031
[0.40, 0.60]	2.136	2.171±0.396±0.054
[0.60, 0.80]	2.741	3.337±0.503±0.085
[0.80, 0.97]	3.495	2.791±0.493±0.070

$e^+e^- \to \mu^+\mu^-$ ($\sqrt{s} \sim 200$ GeV)		
	$d\sigma/d\cos\theta$ (pb)	
$\cos\theta$	Theory	Measurement
[-0.97,-0.80]	0.440	0.560±0.211±0.016
[-0.80,-0.60]	0.435	0.266±0.133±0.007
[-0.60,-0.40]	0.498	0.885±0.236±0.023
[-0.40,-0.20]	0.639	0.699±0.211±0.018
[-0.20, 0.00]	0.860	1.053±0.263±0.029
[0.00, 0.20]	1.165	1.301±0.291±0.035
[0.20, 0.40]	1.556	1.694±0.326±0.044
[0.40, 0.60]	2.037	2.957±0.436±0.079
[0.60, 0.80]	2.615	2.877±0.439±0.079
[0.80, 0.97]	3.338	3.656±0.533±0.099

$e^+e^- \to \mu^+\mu^-$ ($\sqrt{s} \sim 202$ GeV)		
	$d\sigma/d\cos\theta$ (pb)	
$\cos\theta$	Theory	Measurement
[-0.97,-0.80]	0.435	1.077±0.407±0.029
[-0.80,-0.60]	0.429	0.585±0.292±0.017
[-0.60,-0.40]	0.489	0.259±0.183±0.007
[-0.40,-0.20]	0.625	0.249±0.176±0.007
[-0.20, 0.00]	0.841	0.392±0.226±0.011
[0.00, 0.20]	1.138	0.515±0.257±0.014
[0.20, 0.40]	1.518	2.385±0.562±0.065
[0.40, 0.60]	1.988	1.325±0.419±0.036
[0.60, 0.80]	2.552	2.051±0.530±0.057
[0.80, 0.97]	3.259	3.125±0.717±0.088

Table 5: The differential cross–sections for $\mu^+\mu^-$ and final states at centre–of–mass energies from $\sim$ 192 to 202 GeV. The errors shown are respectively the statistical and systematic components. The Standard Model expectations (SM) were computed with the ZFITTER program [13].

$e^+e^- \to \tau^+\tau^-$ ($\sqrt{s} \sim 192$ GeV)		
	$d\sigma/d\cos\theta$ (pb)	
$\cos\theta$	Theory	Measurement
[-0.96,-0.80]	0.470	0.700±0.770±0.060
[-0.80,-0.60]	0.470	0.310±0.480±0.050
[-0.60,-0.40]	0.550	0.490±0.430±0.060
[-0.40,-0.20]	0.710	0.500±0.500±0.070
[-0.20, 0.00]	0.970	0.940±0.600±0.090
[0.00, 0.20]	1.310	1.220±0.680±0.120
[0.20, 0.40]	1.760	1.600±0.730±0.160
[0.40, 0.60]	2.300	1.510±0.840±0.210
[0.60, 0.80]	2.950	3.450±1.170±0.280
[0.80, 0.96]	3.650	-0.230±1.630±0.310

$e^+e^- \to \tau^+\tau^-$ ($\sqrt{s} \sim 196$ GeV)		
	$d\sigma/d\cos\theta$ (pb)	
$\cos\theta$	Theory	Measurement
[-0.96,-0.80]	0.460	0.700±0.440±0.060
[-0.80,-0.60]	0.460	0.180±0.270±0.050
[-0.60,-0.40]	0.530	0.970±0.250±0.060
[-0.40,-0.20]	0.680	0.690±0.290±0.070
[-0.20, 0.00]	0.920	1.280±0.340±0.090
[0.00, 0.20]	1.250	0.980±0.390±0.120
[0.20, 0.40]	1.670	1.580±0.420±0.160
[0.40, 0.60]	2.190	2.190±0.480±0.210
[0.60, 0.80]	2.810	3.280±0.670±0.280
[0.80, 0.96]	3.480	3.340±0.940±0.310

$e^+e^- \to \tau^+\tau^-$ ($\sqrt{s} \sim 200$ GeV)		
	$d\sigma/d\cos\theta$ (pb)	
$\cos\theta$	Theory	Measurement
[-0.96,-0.80]	0.450	0.100±0.420±0.060
[-0.80,-0.60]	0.450	1.010±0.260±0.050
[-0.60,-0.40]	0.510	0.530±0.240±0.060
[-0.40,-0.20]	0.660	0.530±0.270±0.070
[-0.20, 0.00]	0.880	1.060±0.330±0.090
[0.00, 0.20]	1.200	1.200±0.380±0.120
[0.20, 0.40]	1.600	1.980±0.400±0.160
[0.40, 0.60]	2.090	1.810±0.460±0.210
[0.60, 0.80]	2.820	2.050±0.650±0.280
[0.80, 0.96]	3.320	3.760±0.900±0.310

$e^+e^- \to \tau^+\tau^-$ ($\sqrt{s} \sim 202$ GeV)		
	$d\sigma/d\cos\theta$ (pb)	
$\cos\theta$	Theory	Measurement
[-0.96,-0.80]	0.450	-0.150±0.600±0.060
[-0.80,-0.60]	0.440	0.890±0.380±0.050
[-0.60,-0.40]	0.500	0.450±0.340±0.060
[-0.40,-0.20]	0.640	0.450±0.390±0.070
[-0.20, 0.00]	0.870	1.400±0.480±0.090
[0.00, 0.20]	1.170	0.890±0.540±0.120
[0.20, 0.40]	1.560	2.550±0.580±0.170
[0.40, 0.60]	2.040	2.100±0.670±0.220
[0.60, 0.80]	2.620	1.380±0.930±0.290
[0.80, 0.96]	3.250	2.630±1.290±0.310

Table 6: The differential cross–sections for $\tau^+\tau^-$ and final states at centre–of–mass energies from $\sim$ 192 to 202 GeV. The errors shown are respectively the statistical and systematic components. The Standard Model expectations (SM) were computed with the ZFITTER program [13].

3 Fits to physics beyond the Standard Model

The data presented in this paper were used to improve the constraints on physics beyond the Standard Model given in [2, 3] for three sets of models: contact interactions between leptons, R-parity violating sneutrino exchange, and for models including additional, Z′ bosons. The theoretical bases of each of these models are discussed in section 5 of [2], the key points are summarised below. Limits for models which include gravity in extra dimensions are derived from the measurements of the differential cross–sections, updating the results presented in [3]. Unless otherwise stated, systematic errors for LEP II measurements were added in quadrature with the statistical errors and treated as uncorrelated between measurements.

3.1 Contact interaction models

The parameter fitted was $\epsilon = 1/\Lambda^2$, where Λ is the scale of the interactions in the effective Lagrangian of the four–fermion interactions:

$$\mathcal{L}_{eff} = \frac{g^2}{(1+\delta)\Lambda^2} \sum_{i,j=L,R} \eta_{ij} \overline{e}_i \gamma_\mu e_i \overline{f}_j \gamma^\mu f_j. \quad (1)$$

where the i, j denote either left or right handed helicities of the fermionic currents involved. Different choices of η_{ij} lead to 12 commonly studied models, referred to as LL, RR etc [15]. See sections 5.1 and 6.1.1 of [2] for more details.

A fit for contact interactions between leptons ($e^+e^- \to l^+l^-$) assuming lepton universality in the couplings was made using data at all energies from 130 to 202 GeV for $e^+e^- \to e^+e^-, e^+e^- \to \mu^+\mu^-$ and $e^+e^- \to \tau^+\tau^-$ final states. The values of ϵ extracted for each model were all compatible with the Standard Model expectation $\epsilon = 0$, at the two standard deviation level. The errors on ϵ are typically 75% of those reported in [3] as a result of the inclusion of the new data. The fitted values of ϵ were converted into lower limits on Λ at 95% confidence level, as in [2] The results are given in Table 7.

3.2 Sneutrino exchange

The second set of models consider possible s or t channel sneutrino ($\tilde{\nu}_\ell$) exchange in R-parity violating supersymmetry. The parameters of interest are the dimensionless couplings, λ_{ijk}, between the superfields of different generations, i, j and k, together with the mass of the sneutrino exchanged, $m_{\tilde{\nu}}$. The sneutrino width is not constrained within R-parity violating supersymmetry; a value of 1 GeV has been used [16]. Further details can be found in sections 5.2 and 6.1.2 of [2].

For the $e^+e^- \to \mu^+\mu^-$ and $e^+e^- \to \tau^+\tau^-$ channels, in the case that only one λ value is non–zero there would only be t-channel sneutrino effects. The 95% confidence exclusion upper limits on λ are given in Table 8, assuming sneutrino masses of either 100 or 200 GeV/c^2. The limits are calculated by finding the value of λ for $\chi^2 = \chi^2_{min} + 3.84$. For $e^+e^- \to \mu^+\mu^-$ the limits are 0.29 and 0.40 smaller than those published in [3] for $m_{\tilde{\nu}}$ of 100 and 200 GeV/c^2 respectively.

For the $e^+e^- \to e^+e^-$ channel the resulting 95% limits on λ, are given in Figure 8(a), as a function of $m_{\tilde{\nu}}$. For the fits in the $e^+e^- \to \mu^+\mu^-$ channel, assuming that $\lambda_{131} = \lambda_{232} = \lambda$, the resulting 95% limits on λ are given in Figure 8(b). The exclusion contour

$e^+e^- \to l^+l^-$			
Model	ϵ (TeV^{-2})	Λ^+ (TeV)	Λ^- (TeV)
LL	$-0.005^{+0.006}_{-0.008}$	9.4	7.3
RR	$-0.009^{+0.009}_{-0.006}$	9.0	7.4
VV	$-0.005^{+0.003}_{-0.001}$	17.8	13.6
AA	$0.001^{+0.005}_{-0.002}$	10.2	12.8
RL	$-0.018^{+0.012}_{-0.004}$	8.8	6.4
LR	$-0.018^{+0.012}_{-0.004}$	8.8	6.4

Table 7: Fitted values of ϵ and 95% confidence lower limits on the scale, Λ, of contact interactions in the models discussed in the text for $e^+e^- \to l^+l^-$, a combination of $e^+e^- \to e^+e^-$, $e^+e^- \to \mu^+\mu^-$ and $e^+e^- \to \tau^+\tau^-$ final states in which lepton universality is assumed for the contact interactions.

for $\lambda_{121} = \lambda_{233} = \lambda$, using the $e^+e^- \to \tau^+\tau^-$ channel, is shown in Figure 8(c). In each case, the exclusion contours are calculated by finding the value of λ for $\chi^2 = \chi^2_{min} + 3.84$ for each value of $m_{\tilde{\nu}}$ separately. A coupling of $\lambda > 0.1$ can be excluded for $m_{\tilde{\nu}}$ in the approximate range 130 - 210 GeV/c^2 for all final states, extending the excluded region by approximately 15-20 GeV/c^2 compared to [3].

3.3 Z′-bosons

Existing data from LEP1 and LEP2 and the cross–sections and asymmetries given here were used to fit the data to models including additional Z' bosons.

3.3.1 Model dependent fits

Fits were made to the mass of a Z', $\mathrm{M}_{\mathrm{Z}'}$, the mass of the Z, M_{Z}, and to the mixing angle between the two bosonic fields, $\Theta_{\mathrm{ZZ}'}$, for 4 different models referred to as χ, ψ, η and L-R [17]. More details can be found in section 5.4.1 and 6.3.1 of [2]. The fitted value of M_{Z} was found to be in agreement with the value found from fits to the data with no additional Z'. No evidence was found for the existence of a Z'–boson in any of the models. The 95 % confidence level limits on $\mathrm{M}_{\mathrm{Z}'}$ and $\Theta_{\mathrm{ZZ}'}$ were computed for the different models by determining the contours of the domain in the $\mathrm{M}_{\mathrm{Z}'} - \Theta_{\mathrm{ZZ}'}$ plane where $\chi^2 < \chi^2_{min} + 5.99$ [18]. The allowed regions for $\mathrm{M}_{\mathrm{Z}'}$ and $\Theta_{\mathrm{ZZ}'}$ are shown in Figure 9. The lower limits, shown in Table 9, on the Z' mass range from approximately 320 to 480 GeV/c^2. The limits change by between -28 and +38 GeV/c^2 compared to the limits presented in [3], depending on the model.

For the Sequential Standard Model [20], which proposes the existence of a Z' with exactly the same coupling to fermions as the standard Z, a limit of $\mathrm{M}_{\mathrm{Z}'} > 700\,\mathrm{GeV}/c^2$ is found at 95% confidence. A change of 10 GeV/c^2 on the limit given in [3].

3.3.2 Model independent fits

Fits were performed to the leptonic cross–sections and forward–backward asymmetries, for the leptonic couplings of a Z', $a^N_{l'}$ and $v^N_{l'}$, normalised for the overall coupling scale and the mass of the Z' [19]. See section 5.4.2 and 6.3.2 of [2] for more details.

Several values of the mass of the Z' were considered (i.e. 300, 500 and 1000 GeV/c^2), and the ZZ'–mixing was neglected. The limits on the normalised couplings are $|a^N_{l'}| < 0.20$ and $|v^N_{l'}| < 0.20$, a change of $+0.05$ and -0.02, respectively, on limits given in [3].

3.4 Gravity in Extra Dimensions

Limits on the energy scale $\mathrm{M_s}$ of models of gravity in extra dimensions have been obtained for two cases, $\lambda = \pm 1$, either constructive or destructive interference between the gravitational process and the Standard Model process [21]. For further details refer to section 3.4 of [3].

Fits to the differential cross–sections, $d\sigma/d\cos\theta$, for the parameter $\epsilon = \lambda/\mathrm{M_s^4}$ were performed using data from $\sqrt{s} \sim 192 - 202\,\mathrm{GeV}$, and also including those reported in [3]. Systematic errors correlated between bins for a given channel at a single energy where correctly handled in the fit. The fits gave values compatible with the Standard Model, i.e. $\epsilon = 0$. Table 10 shows the fitted values of ϵ and the 95% confidence level lower limits

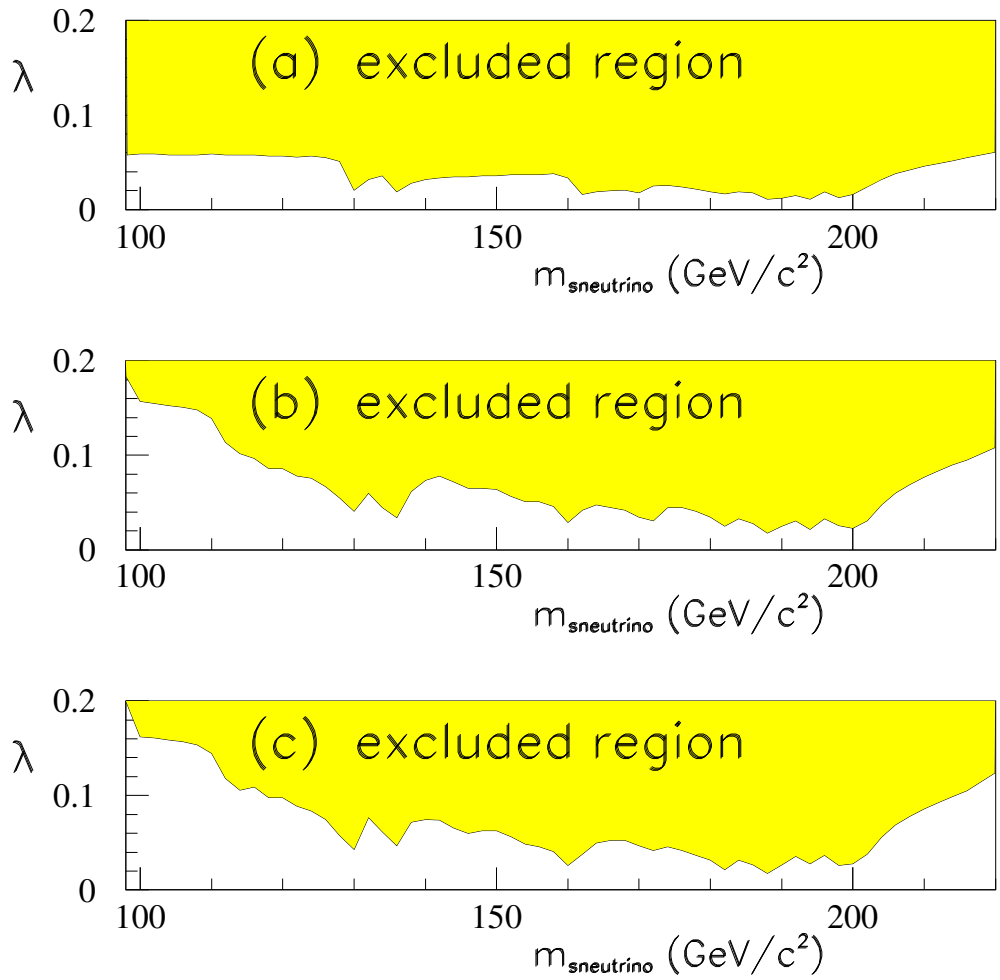

Figure 8: The 95% exclusion limits for (a) λ_{121} (or λ_{131}), as a function of $m_{\tilde{\nu}}$, obtained from the $e^+e^- \to e^+e^-$ channel; (b) $\lambda_{131} = \lambda_{232} = \lambda$, as a function of $m_{\tilde{\nu}}$, obtained from the $e^+e^- \to \mu^+\mu^-$ channel; (c) $\lambda_{121} = \lambda_{233} = \lambda$, as a function of $m_{\tilde{\nu}}$, obtained from the $e^+e^- \to \tau^+\tau^-$ channel. The sneutrino width is taken to be 1 GeV.

coupling	$m_{\tilde{\nu}} = 100\ \mathrm{GeV}/c^2$ (95% c.l.)	$m_{\tilde{\nu}} = 200\ \mathrm{GeV}/c^2$ (95% c.l.)
λ (t-channel $\tilde{\nu}_\ell$ in $e^+e^- \to \mu^+\mu^-$)	0.21	0.28
λ (t-channel $\tilde{\nu}_\ell$ in $e^+e^- \to \tau^+\tau^-$)	0.48	0.66

Table 8: Upper limits on the couplings λ in t channel sneutrino exchange in $e^+e^- \to \mu^+\mu^-$ and $e^+e^- \to \tau^+\tau^-$ for sneutrino masses of 100 and 200 GeV/c^2. The couplings involved are given in the text.

Figure 9: The allowed domain in the $M_{Z'} - \Theta_{ZZ'}$ plane for the χ, ψ, η and L-R models. The contours show the 95% confidence level limits.

Model	χ	ψ	η	L-R
$M_{Z'}^{limit}$ (GeV/c^2)	478	322	335	375
$\mid \Theta_{ZZ'}^{limit} \mid$ (mrad)	1.6	2.0	2.3	1.9

Table 9: 95% confidence level lower limits on the Z$'$ mass and upper limits on the ZZ$'$ mixing angle within the χ, ψ, η and L-R models.

Final State	$\sqrt{s}$ (GeV)	ϵ_{Best} (TeV^{-4})	λ	M_S(TeV)
$\mu^+\mu^-$	$192-202$	$-4.32^{+2.98}_{-2.73}$	-1	0.581
			$+1$	0.680
	$183-202$	$-4.84^{+2.39}_{-2.02}$	-1	0.592
			$+1$	0.725
$\tau^+\tau^-$	$192-202$	$+0.67^{+4.33}_{-4.26}$	-1	0.614
			$+1$	0.599
	183-202	$-4.49^{+3.46}_{-3.59}$	-1	0.557
			$+1$	0.645
l^+l^-	$192-202$	$-2.77^{+2.39}_{-2.37}$	-1	0.623
			$+1$	0.711
	$183-202$	$-4.39^{+2.10}_{-1.65}$	-1	0.598
			$+1$	0.755

Table 10: 95% confidence level lower limits on M_s in models of gravity in extra dimensions for $\mu^+\mu^-$ and $\tau^+\tau^-$ final states, and for l^+l^-, a combination of both muon and tau final states.

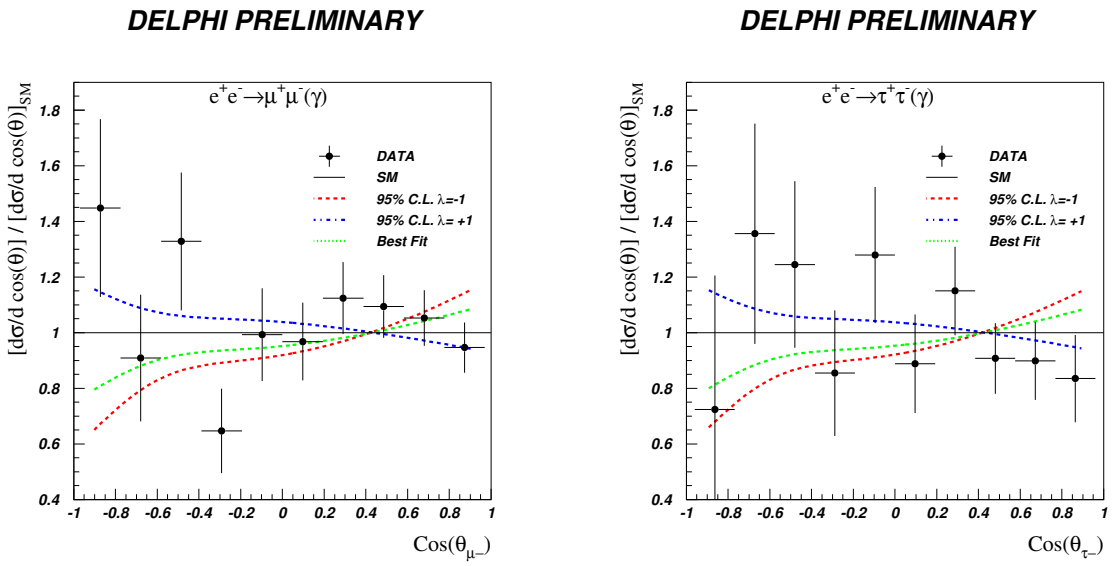

Figure 10: The weighted average of the deviations from the Standard Model angular distributions for measurements at $\sqrt{s} \sim 192-202$ GeV for $\mu^+\mu^-$ and $\tau^+\tau^-$ final states. Superimposed are the deviations expected from the effects of gravity in extra dimensions calculated at the combined limits for both channels and all energies for $\lambda = \pm 1$, and evaluated at the mean centre of mass energy of the data.

on M_s. These limits were obtained using a method equivalent to that used to extract the limits on the scale, Λ, of contact interactions, as described in section 6.1.1 of [2]. The deviations in the differential cross–sections for models of gravity in extra dimensions are compared to the data in Figure 10.

4 Summary and conclusions

The results of the analyses of cross–sections and asymmetries at $\sqrt{s} \sim 192 - 202$ GeV in the channels $e^+e^- \to e^+e^-(\gamma)$, $e^+e^- \to \mu^+\mu^-(\gamma)$, $e^+e^- \to \tau^+\tau^-(\gamma)$ and inclusive $e^+e^- \to q\bar{q}(\gamma)$, have been presented.

Overall, the data agree with the Standard Model predictions of ZFITTER and TOPAZ0. The data were used to update the searches for physics beyond the Standard Model given in [2, 3] and to investigate the possible effects of gravity in extra dimensions given in [3]. No evidence for physics beyond the Standard Model was found, and limits were set on parameters of several more general models. The scale Λ characterising contact interactions between all leptons can be excluded at 95% confidence level in the range $\Lambda < 6.4 - 17.8$ TeV depending on the model. For sneutrino exchange in R-parity violating supersymmetry, values of the the generic coupling in the purely leptonic part of the superpotential, $\lambda > 0.1$ can be excluded for $m_{\tilde{\nu}}$ in the range 130 - 210 GeV for all leptonic states at the 95% confidence level or above. Alternatively, Z' bosons lighter than $\sim 320\,\mathrm{GeV}/^2$ can be excluded at the 95% confidence level in the models considered. Lastly, 95% confidence level lower limits of 598 and 755 GeV on the string scale, M_s, for $\lambda = -1$ and $\lambda = +1$ respectively, in models of gravity involving extra dimensions are obtained for a combinations of $\mu^+\mu^-$ and $\tau^+\tau^-$ final states.

Acknowledgements

We thank the SL Division of CERN for the excellent performance of the LEP collider and our funding agencies.

References

[1] DELPHI Collaboration, P. Aarnio *et al.* , Nucl. Instr. & Meth. **A303** (1991) 233.
DELPHI Collaboration, P. Abreu *et al.* , Nucl. Instr. & Meth. **A378** (1996) 57.

[2] DELPHI Collaboration, P. Abreu *et al.* , Eur.Phys.J. **C11** (1999) 383.

[3] DELPHI Collaboration, P. Abreu *et al.* CERN-EP/2000-068

[4] DELPHI Collaboration, P. Abreu *et al.* , Nucl. Phys. **B417** (1994) 3.

[5] DELPHI Collaboration, P. Abreu *et al.* , Nucl. Phys. **B418** (1994) 403.
DELPHI Collaboration, in preparation.

[6] ALEPH Collaboration, D. Buskulic *et al.* , Phys. Lett. **B378** (1996) 373;
ALEPH Collaboration, R. Barate *et al.* , Phys. Lett. **B399** (1997) 329;
ALEPH Collaboration, R. Barate *et al.* , Euro. Phys. J. **C12** (2000) 183;

L3 Collaboration, M. Acciarri *et al.* , Phys. Lett. **B370** (1996) 195;
L3 Collaboration, M. Acciarri *et al.* , Phys. Lett. **B407** (1997) 361;
L3 Collaboration, M. Acciarri *et al.* , Phys. Lett. **B433** (1998) 163;
L3 Collaboration, M. Acciarri *et al.* , Phys. Lett. **B464** (1999) 135;
L3 Collaboration, M. Acciarri *et al.* , Phys. Lett. **B470** (1999) 281;
L3 Collaboration, M. Acciarri *et al.* , Phys. Lett. **B479** (2000) 101;
OPAL Collaboration, K. Ackerstaff *et al.* , Euro. Phys. J. **C2** (1998) 441;
OPAL Collaboration, G. Abbiendi *et al.* , Euro. Phys. J. **C6** (1999) 1;
OPAL Collaboration, G. Abbiendi *et al.* , Euro. Phys. J. **C13** (2000) 553;

[7] LEP Energy Working Group 99-01
CERN-EP/98-191

[8] T. Sjöstrand, PYTHIA 5.7/JETSET 7.4 CERN-TH 7112/93 (1993)

[9] F. A. Berends, R. Pittau and R. Kliess, Comp. Phys. Comm. **85** (1995) 437.

[10] S. Nova *et al.* , DELPHI Note 90-35.

[11] F. A. Berends, P. H. Daverveldt and R. Klies, Comp. Phys. Comm. **40** (1986) 271.

[12] S. Jadach, B.F.L. Ward and Z. Was, Comp. Phys. Comm. **79** (1994) 503.

[13] D. Bardin *et al.* , *"ZFITTER: An Analytical Program for Fermion Pair Production in e^+e^- Annihilation"*, HEP-PH/9908433 (1999)

[14] G. Montagna *et al.* , Nucl. Phys. **B401** (1993) 3;
G. Montagna *et al.* , Comput. Phys. Commun. **76** (1993) 328.

[15] E. Eichten, K. Lane and M. Peskin, Phys. Rev. Lett. **50** (1983) 811.

[16] J. Kalinowski *et al.* , Zeit. Phys. **C74** (1997) 595.

[17] P. Langacker, R.W. Robinett and J.L. Rosner, Phys. Rev. **D30** (1984) 1470;
D. London and J.L. Rosner, Phys. Rev. **D34** (1986) 1530;
J.C. Pati and A. Salam, Phys. Rev. **D10** (1974) 275;
R.N. Mohapatra and J.C. Pati, Phys. Rev. **D11** (1975) 566.

[18] F. James, *"MINUIT Reference Manual"*, CERN Program Library Long Writeup D506 (1994)

[19] A. Leike, Zeit. Phys. **C62** (1994) 265.

[20] G. Altarelli *et al.* , Z. Phys. C45 (1989) 109;
erratum Z. Phys. C47 (1990) 676.

[21] N. Arkani-Hamed *et al.* , Phys. Rev. **D59** (1999) 086004.
J. L. Hewett, Phys. Rev. Lett. **82** (1999) 4765.
Gian F. Giudice *et al.* , Nucl. Phys. **B544** (1999) 3.